

**Journal of
Mechanics of
Materials and Structures**

**ELASTIC WAVE PROPAGATION IN A PERIODIC COMPOSITE
PLATE STRUCTURE: BAND GAPS INCORPORATING MICROSTRUCTURE,
SURFACE ENERGY AND FOUNDATION EFFECTS**

Gongye Zhang and Xin-Lin Gao

Volume 14, No. 2

March 2019



ELASTIC WAVE PROPAGATION IN A PERIODIC COMPOSITE PLATE STRUCTURE: BAND GAPS INCORPORATING MICROSTRUCTURE, SURFACE ENERGY AND FOUNDATION EFFECTS

GONGYE ZHANG AND XIN-LIN GAO

A new model for predicting band gaps for flexural elastic wave propagation in a periodic composite plate structure is developed using a non-classical Kirchhoff plate model that is based on a modified couple stress theory, a surface elasticity theory and a two-parameter Winkler–Pasternak elastic foundation model. The formulation is based on the plane wave expansion method and Bloch’s theorem. The current non-classical model simultaneously incorporates microstructure, surface energy and foundation effects, unlike existing models. When the microstructure and surface energy effects are both suppressed, the new model reduces to the classical elasticity-based model. The band gaps predicted by the newly developed model vary with the microstructure-dependent length scale parameters, the surface elastic constants, the elastic foundation moduli, the unit cell size, and the volume fraction. The numerical results reveal that the first band gap including the foundation effect is always smaller than that without considering the foundation effect, and the first foundation band gap size increases with the increase of the elastic foundation moduli. Also, the first band gap predicted by the new non-classical model is always larger than that predicted by the classical model, but the difference is diminishing as the plate thickness increases. In addition, it is found that the sizes of the first band gap and the first foundation band gap decrease with the increase of the unit cell length at different length scales. Furthermore, it is seen that the volume fraction has a significant effect on the sizes of the first band gap and the first foundation band gap, and band gaps can be tailored by adjusting the volume fraction as well as the constituent properties.

1. Introduction

Band gaps for elastic wave propagation in periodic composite beam and plate structures have received increasing attention (e.g., Sigalas and Economou 1994; Liu and Hussein 2012; Xiao et al. 2012; Piccolroaz and Movchan 2014; Zhang and Parnell 2017; Piccolroaz et al. 2017; Chen et al. 2017; Zhang et al. 2018a). Such periodic composite structures can generate band gaps and are therefore good candidate materials for filtering waves, isolating vibrations and harvesting energy. Bragg scattering and local resonance, two leading causes for band gaps (e.g., Liu and Hussein 2012; Chen and Wang 2014; Madeo et al. 2016), can both be present in such composite structures.

Thin beams and plates often exhibit size effects at the micron and nanometer scales. Microstructure- and/or surface energy-dependent length scale effects have been computationally demonstrated through atomistic simulations for amorphous silica and polymers [Maranganti and Sharma 2007], FCC metals including Ni, Cu and Al [Shodja et al. 2012] and noncoherent metallic bicrystals [Mi et al. 2008]. Recently,

Keywords: band gaps, wave propagation, Kirchhoff plate, couple stress, surface elasticity, elastic foundation, plane wave expansion method, Bloch theorem, size effect.

it has been shown that such nonlocal effects can also be experimentally measured with high accuracy by using the shifts of resonant frequencies of a micron- or nanometer-sized beam [Zhang and Zhao 2016].

Band gap generation is inherently related to material microstructures, and hence band gaps for elastic wave propagation in micro- or nano-structured composite beams and plates are also size-dependent, which cannot be described by applying wave equations based on classical elasticity. As a result, wave equations derived through using non-classical elasticity theories containing material length scale parameters need to be employed in determining band gaps at the micron and nanometer scales.

Several non-classical/high-order elasticity theories have been applied to derive wave equations and study band gaps. Liu et al. [2012] used wave equations based on the surface elasticity theory [Gurtin and Murdoch 1975; 1978] to investigate surface energy effects on band gaps. Li et al. [2016] studied band gaps by employing the wave equations built upon the simplified strain gradient elasticity theory (e.g., Gao and Park 2007). Madeo et al. [2016] applied the wave equations based on a relaxed micromorphic elasticity theory to explore frequency band gaps in metamaterials. Bacigalupo and Gambarotta [2017] utilized a micropolar continuum theory to study band gaps in periodic materials. Band gaps for flexural elastic wave propagation in periodic composite beam structures were recently studied by Zhang et al. [2018a] and Gao et al. [2018] by using non-classical Bernoulli–Euler and Timoshenko beam models based on a modified couple stress theory [Yang et al. 2002; Park and Gao 2008] and a surface elasticity theory [Gurtin and Murdoch 1975; 1978; Steigmann and Ogden 1997; 1999]. However, wave equations for plates built upon such higher-order elasticity theories have not been utilized to determine band gaps in periodic composite plate structures. This motivated the present study.

In the current paper, band gaps for flexural elastic wave propagation in a periodic composite plate structure are studied by using a non-classical Kirchhoff plate model based on the modified couple stress theory [Yang et al. 2002; Park and Gao 2008], the surface elasticity theory [Gurtin and Murdoch 1975; 1978] and a two-parameter Winkler–Pasternak elastic foundation model. In Section 2, the equations of motion for a Kirchhoff plate incorporating the microstructure, surface energy and foundation effects derived by Gao and Zhang [2016] are applied to the current periodic composite plate structure to study wave propagation. The formulation is enabled by using the plane wave expansion method and Bloch’s theorem. In Section 3, numerical results for the band gaps predicted by the current non-classical model are presented and compared to those based on the classical elasticity-based model. A summary is provided in Section 4.

2. Formulation

Based on the modified couple stress theory [Yang et al. 2002; Park and Gao 2008], the surface elasticity theory [Gurtin and Murdoch 1975; 1978; Steigmann and Ogden 1997; 1999] and a two-parameter Winkler–Pasternak elastic foundation model (e.g., Yokoyama 1996), the equations of motion for a Kirchhoff plate were derived by Gao and Zhang [2016], which incorporate the microstructure, surface energy and elastic foundation effects. When only the deflection is considered (i.e., $w = w(x, y, t)$, $u = 0$, $v = 0$), the equations of motion reduce to

$$-\left[\frac{1}{12}(\lambda + 2\mu)h^3 + \mu l^2 h + \frac{1}{2}(\lambda_0 + 2\mu_0)h^2\right](w_{,xxxx} + 2w_{,xxyy} + w_{,yyyy}) + (2\tau_0 + k_p)(w_{,xx} + w_{,yy}) - k_w w + f_z - c_{x,y} + c_{y,x} = m_0 \ddot{w} - m_2 \frac{\partial^2 \ddot{w}}{\partial x^2} - m_2 \frac{\partial^2 \ddot{w}}{\partial y^2}, \quad (1a)$$

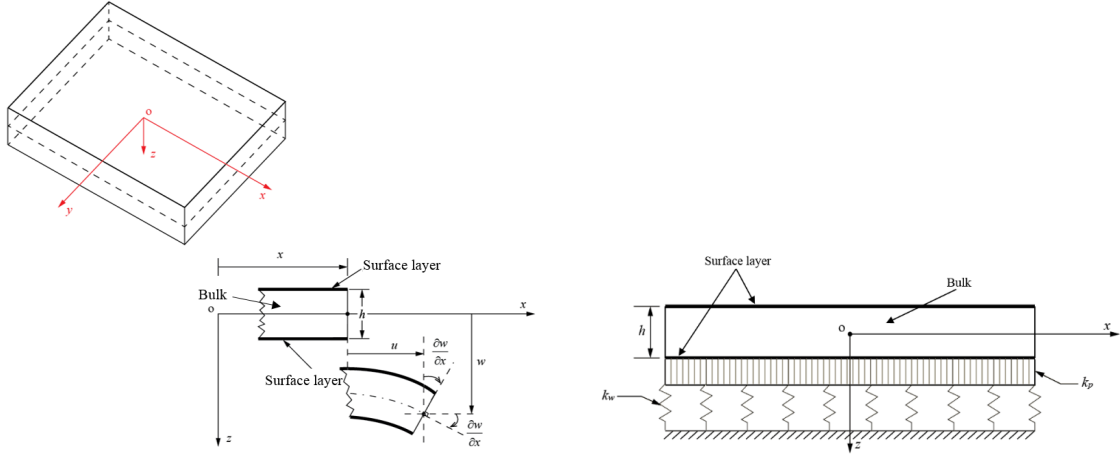


Figure 1. Left: plate configuration and coordinate system. Right: plate on a two-parameter elastic foundation.

which can be rewritten as

$$\begin{aligned}
 & -\frac{\partial^2}{\partial x^2} \left(D \frac{\partial^2 w}{\partial x^2} + C \frac{\partial^2 w}{\partial y^2} \right) - \frac{\partial^2}{\partial y^2} \left(D \frac{\partial^2 w}{\partial y^2} + C \frac{\partial^2 w}{\partial x^2} \right) - \frac{\partial^2}{\partial x \partial y} \left(B \frac{\partial^2 w}{\partial x \partial y} \right) + \frac{\partial}{\partial x} \left(S \frac{\partial w}{\partial x} \right) + \frac{\partial}{\partial y} \left(S \frac{\partial w}{\partial y} \right) \\
 & - k_w w + k_p \left(\frac{\partial^2 w}{\partial x^2} + \frac{\partial^2 w}{\partial y^2} \right) + f_z - c_{x,y} + c_{y,x} = \frac{\partial^2}{\partial t^2} (P_1 w) - \frac{\partial^2}{\partial t^2} \left(P_2 \frac{\partial^2 w}{\partial x^2} \right) - \frac{\partial^2}{\partial t^2} \left(P_2 \frac{\partial^2 w}{\partial y^2} \right), \quad (1b)
 \end{aligned}$$

where $w = w(x, y, t)$ is the displacement in the z -direction (or deflection) of point $(x, y, 0)$ on the plate mid-plane at time t (see Figure 1, left), and

$$\begin{aligned}
 D &= \frac{1}{12}(\lambda + 2\mu)h^3 + \mu l^2 h + \frac{1}{2}(\lambda_0 + 2\mu_0)h^2, & C &= \frac{1}{12}h^3 \lambda - \mu l^2 h + \frac{1}{2}h^2(\lambda_0 + \tau_0), \\
 B &= \frac{1}{3}\mu h^3 + 4\mu l^2 h + h^2(2\mu_0 - \tau_0), & S &= 2\tau_0, & P_1 &= \rho h, & P_2 &= \frac{1}{12}\rho h^3.
 \end{aligned} \quad (2)$$

In (1a), (1b) and (2), λ and μ are the Lamé constants, l is a couple stress-related material length scale parameter (e.g., Mindlin 1963; Park and Gao 2006), μ_0 , λ_0 and τ_0 are the surface elastic constants, ρ is the density of the plate material, h is the uniform plate thickness, f_z is the z -component of the body force resultant (force per unit area) through the plate thickness acting on the plate mid-plane occupying the area R , c_x and c_y are, respectively, the x - and y -components of the body couple resultant (moment per unit area), k_w is the Winkler foundation modulus, and k_p is the Pasternak foundation modulus (e.g., Yokoyama 1996). The plate on the two-parameter elastic foundation is schematically shown in Figure 1 (right).

Note that in deriving the equations of motion leading to (1a), the modified couple stress theory [Yang et al. 2002; Park and Gao 2008] is used for the bulk plate material, and the surface elasticity theory [Gurtin and Murdoch 1975; 1978] is applied to the surface layers (with zero-thickness), which have distinct properties and are perfectly bonded to the bulk plate. When both the microstructure and surface energy effects are suppressed by setting $l = c_x = c_y = 0$ and $\lambda_0 = \mu_0 = \tau_0 = 0$, equation (1a) reduces to

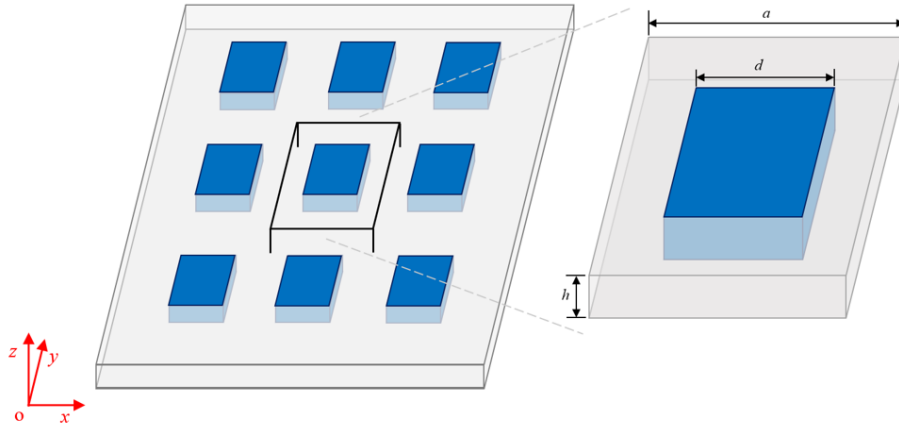


Figure 2. Periodic two-phase composite plate structure with a through-thickness square inclusion phase and a matrix phase: the composite plate structure (left) and the unit cell (right).

the equation of motion for a Kirchhoff plate resting on the Winkler–Pasternak elastic foundation based on classical elasticity.

Consider a periodic two-phase composite plate structure containing through-thickness square inclusions (as Phase *I*) embedded periodically in a host matrix (as Phase *II*), as shown in Figure 2. The periodic composite structure is infinitely large in the xy -plane. The unit cell for this periodic composite plate structure with a uniform thickness h is taken to be a square (with edge length a) containing a square inclusion (with edge length d) at its center, as displayed in Figure 3. The corresponding irreducible first Brillouin zone is also shown in Figure 3.

For the current periodic composite plate structure, the plane wave expansion method (e.g., Sigalas 1997) and Bloch’s theorem for periodic media (e.g., Kittel 1986) can be applied. Accordingly, the deflection w can be expanded in a Fourier series as (e.g., Zhang et al. 2018b; Zhang and Gao 2018):

$$w(\mathbf{r}, t) = e^{i\mathbf{k}\cdot\mathbf{r}} \left(\sum_{\mathbf{G}'_{(m,n)}} w_{\mathbf{G}'_{(m,n)}} e^{i\mathbf{G}'_{(m,n)}\cdot\mathbf{r}} \right) e^{-i\omega t}, \quad (3)$$

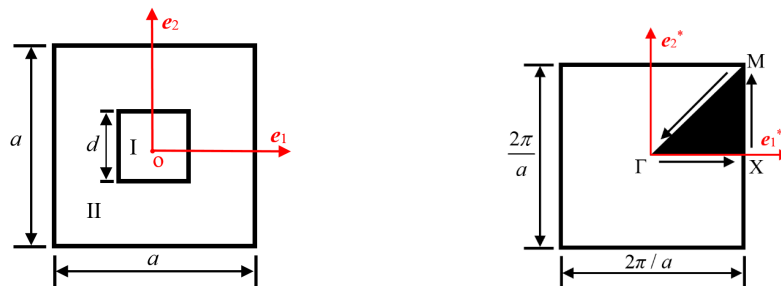


Figure 3. Left: unit cell of the periodic composite plate with a square inclusion (phase *I*). Right: the irreducible first Brillouin zone in the reciprocal lattice.

where $w_{\mathbf{G}'_{(m,n)}}$ is the Fourier coefficient, $\mathbf{r} = (x, y)$ is the position vector, $\mathbf{k} = (k_x, k_y)$ is the Bloch wave vector, $\mathbf{G}'_{(m,n)} = (2\pi m/a, 2\pi n/a) = (G'_x, G'_y)$ is the reciprocal lattice vector for a square lattice, ω is the angular frequency, i is the imaginary unit satisfying $i^2 = -1$, m and n are integers ranging from $-\infty$ to $+\infty$, and a is the lattice constant that is equal to the unit cell edge length (see Figure 3).

In addition, based on the periodicity of the composite plate structure, $D(\mathbf{r})$, $C(\mathbf{r})$, $B(\mathbf{r})$, $S(\mathbf{r})$, $P_1(\mathbf{r})$, $P_2(\mathbf{r})$, $k_w(\mathbf{r})$ and $k_p(\mathbf{r})$, which are material parameters involved in the wave equation in (1b), can each be written as a Fourier series:

$$\alpha(\mathbf{r}) = \sum_{\mathbf{G}_{(M,N)}} \alpha_{\mathbf{G}_{(M,N)}} e^{i\mathbf{G}_{(M,N)} \cdot \mathbf{r}}, \quad (4)$$

where α denotes D , C , B , S , P_1 , P_2 , k_w or k_p , $\mathbf{G}_{(M,N)} = (2\pi M/a, 2\pi N/a) = (G_x, G_y)$ is the reciprocal lattice vector in which the integers M and N range from $-\infty$ to $+\infty$, and $\alpha_{\mathbf{G}}$ is the Fourier coefficient satisfying

$$\alpha_{\mathbf{G}_{(M,N)}} = \frac{1}{A} \iint_{\Omega} \alpha(\mathbf{r}) e^{-i\mathbf{G}_{(M,N)} \cdot \mathbf{r}} d\mathbf{r}, \quad (5)$$

where Ω is the square domain on the plate mid-plane in the unit cell, and A is the area of Ω . It can be readily shown that for a two-phase composite, $\alpha_{\mathbf{G}}$ is given by

$$\alpha_{\mathbf{G}} = \begin{cases} V_f^{(I)} \alpha_I + (1 - V_f^{(I)}) \alpha_{II} & \text{when } \mathbf{G}_{(M,N)} = \mathbf{0}, \\ (\alpha_I - \alpha_{II}) F(\mathbf{G}_{(M,N)}) & \text{when } \mathbf{G}_{(M,N)} \neq \mathbf{0}, \end{cases} \quad (6)$$

where α_I and α_{II} are respective property values for materials I and II , $V_f^{(I)}$ is the volume fraction of the inclusion phase (material I) given by $V_f^{(I)} = A^{(I)}/A$ (with $A^{(I)}$ being the mid-plane area of material I in the unit cell), and $F(\mathbf{G}_{(M,N)})$ is the shape function defined by

$$F(\mathbf{G}_{(M,N)}) = \frac{1}{A} \iint_{\Omega_I} e^{-i\mathbf{G}_{(M,N)} \cdot \mathbf{r}} d\mathbf{r}, \quad (7)$$

where Ω_I is the mid-plane domain occupied by material I in the unit cell.

For a square inclusion occupying the domain Ω_I (see Figure 3, left), $F(\mathbf{G}_{(M,N)})$ is given by (e.g., Susa 2002):

$$F(\mathbf{G}_{(M,N)}) = \begin{cases} \frac{2d}{a^2 G_x} \sin \frac{G_x d}{2} & \text{for } G_x \neq 0, G_y = 0, \\ \frac{2d}{a^2 G_y} \sin \frac{G_y d}{2} & \text{for } G_x = 0, G_y \neq 0, \\ \frac{4}{a^2 G_x G_y} \sin \frac{G_x d}{2} \sin \frac{G_y d}{2} & \text{for } G_x \neq 0, G_y \neq 0, \end{cases} \quad (8)$$

where d and a are, respectively, the edge lengths of the square inclusion Ω_I and unit cell Ω shown in Figure 3 (left).

Using (3) and (4) in (1b) (with $f_z = c_x = c_y = 0$) yields

$$(\mathbf{M})_{\mathbf{G}_{(M,N)} - \mathbf{G}'_{(m,n)}} w_{\mathbf{G}'_{(m,n)}} = \omega^2 (\mathbf{R})_{\mathbf{G}_{(M,N)} - \mathbf{G}'_{(m,n)}} w_{\mathbf{G}'_{(m,n)}}, \quad (9)$$

where

$$\begin{aligned}
(M)_{\mathbf{G}_{(M,N)}-\mathbf{G}'_{(m,n)}} &= D_{\mathbf{G}-\mathbf{G}'}(k_x + G_x)^2(k_x + G'_x)^2 + C_{\mathbf{G}-\mathbf{G}'}(k_x + G_x)^2(k_y + G'_y)^2 \\
&\quad + D_{\mathbf{G}-\mathbf{G}'}(k_y + G_y)^2(k_y + G'_y)^2 + C_{\mathbf{G}-\mathbf{G}'}(k_y + G_y)^2(k_x + G'_x)^2 \\
&\quad + B_{\mathbf{G}-\mathbf{G}'}(k_x + G_x)(k_y + G_y)(k_x + G'_x)(k_y + G'_y) \\
&\quad + S_{\mathbf{G}-\mathbf{G}'}(k_x + G_x)(k_x + G'_x) + S_{\mathbf{G}-\mathbf{G}'}(k_y + G_y)(k_y + G'_y) \\
&\quad + (k_w)_{\mathbf{G}-\mathbf{G}'} + (k_p)_{\mathbf{G}-\mathbf{G}'}(k_x + G'_x)^2 + (k_p)_{\mathbf{G}-\mathbf{G}'}(k_y + G'_y)^2, \tag{10}
\end{aligned}$$

$$(R)_{\mathbf{G}_{(M,N)}-\mathbf{G}'_{(m,n)}} = (P_1)_{\mathbf{G}-\mathbf{G}'} + (P_2)_{\mathbf{G}-\mathbf{G}'}(k_x + G'_x)^2 + (P_2)_{\mathbf{G}-\mathbf{G}'}(k_y + G'_y)^2, \tag{11}$$

$$w_{\mathbf{G}'_{(m,n)}} = \frac{1}{A} \iint_{\Omega} w e^{-i(\mathbf{G}'_{(m,n)}+\mathbf{k})\cdot\mathbf{r}} d\mathbf{r}, \tag{12}$$

in which

$$\alpha_{\mathbf{G}-\mathbf{G}'} = \frac{1}{A} \iint_{\Omega} \alpha e^{-i(\mathbf{G}_{(M,N)}-\mathbf{G}'_{(m,n)})\cdot\mathbf{r}} d\mathbf{r}, \tag{13}$$

where $\alpha_{\mathbf{G}-\mathbf{G}'}$ represents $D_{\mathbf{G}-\mathbf{G}'}$, $C_{\mathbf{G}-\mathbf{G}'}$, $B_{\mathbf{G}-\mathbf{G}'}$, $S_{\mathbf{G}-\mathbf{G}'}$, $(P_1)_{\mathbf{G}-\mathbf{G}'}$, $(P_2)_{\mathbf{G}-\mathbf{G}'}$, $(k_w)_{\mathbf{G}-\mathbf{G}'}$ or $(k_p)_{\mathbf{G}-\mathbf{G}'}$. Note that in reaching (9), use has been made of Laurent's rule for finding the Fourier coefficients of a product of two periodic functions (e.g., Li 1996; Cao et al. 2004).

When each of the integers m , n , M , and N in the Fourier series expansions for w and α (representing D , C , B , S , P_1 , P_2 , k_w or k_p) given in (3) and (4) is set to range from $-L$ to L , equation (9) leads to $(2L + 1)^2$ equations, which can be written as

$$[(M)_{\mathbf{G}-\mathbf{G}'}]\{w_{\mathbf{G}'}\} = \omega^2[(R)_{\mathbf{G}-\mathbf{G}'}]\{w_{\mathbf{G}'}\}, \tag{14}$$

where

$$[(M)_{\mathbf{G}-\mathbf{G}'}] = \begin{bmatrix} M_{(\mathbf{G}_{(-L,-L)}-\mathbf{G}'_{(-L,-L)})} & M_{(\mathbf{G}_{(-L,-L)}-\mathbf{G}'_{(-L,-L+1)})} & \cdots & M_{(\mathbf{G}_{(-L,-L)}-\mathbf{G}'_{(L,L-1)})} & M_{(\mathbf{G}_{(-L,-L)}-\mathbf{G}'_{(L,L)})} \\ M_{(\mathbf{G}_{(-L,-L+1)}-\mathbf{G}'_{(-L,-L)})} & M_{(\mathbf{G}_{(-L,-L+1)}-\mathbf{G}'_{(-L,-L+1)})} & \cdots & M_{(\mathbf{G}_{(-L,-L+1)}-\mathbf{G}'_{(L,L-1)})} & M_{(\mathbf{G}_{(-L,-L+1)}-\mathbf{G}'_{(L,L)})} \\ \vdots & \vdots & \vdots & \vdots & \vdots \\ M_{(\mathbf{G}_{(L,L-1)}-\mathbf{G}'_{(-L,-L)})} & M_{(\mathbf{G}_{(L,L-1)}-\mathbf{G}'_{(-L,-L+1)})} & \cdots & M_{(\mathbf{G}_{(L,L-1)}-\mathbf{G}'_{(L,L-1)})} & M_{(\mathbf{G}_{(L,L-1)}-\mathbf{G}'_{(L,L)})} \\ M_{(\mathbf{G}_{(L,L)}-\mathbf{G}'_{(-L,-L)})} & M_{(\mathbf{G}_{(L,L)}-\mathbf{G}'_{(-L,-L+1)})} & \cdots & M_{(\mathbf{G}_{(L,L)}-\mathbf{G}'_{(L,L-1)})} & M_{(\mathbf{G}_{(L,L)}-\mathbf{G}'_{(L,L)})} \end{bmatrix}, \tag{15}$$

$$[(R)_{\mathbf{G}-\mathbf{G}'}] = \begin{bmatrix} R_{(\mathbf{G}_{(-L,-L)}-\mathbf{G}'_{(-L,-L)})} & R_{(\mathbf{G}_{(-L,-L)}-\mathbf{G}'_{(-L,-L+1)})} & \cdots & R_{(\mathbf{G}_{(-L,-L)}-\mathbf{G}'_{(L,L-1)})} & R_{(\mathbf{G}_{(-L,-L)}-\mathbf{G}'_{(L,L)})} \\ R_{(\mathbf{G}_{(-L,-L+1)}-\mathbf{G}'_{(-L,-L)})} & R_{(\mathbf{G}_{(-L,-L+1)}-\mathbf{G}'_{(-L,-L+1)})} & \cdots & R_{(\mathbf{G}_{(-L,-L+1)}-\mathbf{G}'_{(L,L-1)})} & R_{(\mathbf{G}_{(-L,-L+1)}-\mathbf{G}'_{(L,L)})} \\ \vdots & \vdots & \vdots & \vdots & \vdots \\ R_{(\mathbf{G}_{(L,L-1)}-\mathbf{G}'_{(-L,-L)})} & R_{(\mathbf{G}_{(L,L-1)}-\mathbf{G}'_{(-L,-L+1)})} & \cdots & R_{(\mathbf{G}_{(L,L-1)}-\mathbf{G}'_{(L,L-1)})} & R_{(\mathbf{G}_{(L,L-1)}-\mathbf{G}'_{(L,L)})} \\ R_{(\mathbf{G}_{(L,L)}-\mathbf{G}'_{(-L,-L)})} & R_{(\mathbf{G}_{(L,L)}-\mathbf{G}'_{(-L,-L+1)})} & \cdots & R_{(\mathbf{G}_{(L,L)}-\mathbf{G}'_{(L,L-1)})} & R_{(\mathbf{G}_{(L,L)}-\mathbf{G}'_{(L,L)})} \end{bmatrix} \tag{16}$$

are two $(2L+1)^2 \times (2L+1)^2$ matrices, and

$$\{w_{G'}\} = \begin{Bmatrix} w_{G'(-L,-L)} \\ w_{G'(-L,-L+1)} \\ \vdots \\ w_{G'(L,L-1)} \\ w_{G'(L,L)} \end{Bmatrix} \quad (17)$$

is a $(2L+1)^2 \times 1$ matrix.

For the linear system of equations in (14) to have a nontrivial solution of $w_{G'_{(m,n)}} \neq 0$, the determinant of the coefficient matrix must vanish, which gives

$$|[T] - \omega^2[I]| = 0, \quad (18)$$

as the characteristic equation of the eigenvalue problem defined in (14), where

$$[T] = [(R)_{G-G'}]^{-1}[(M)_{G-G'}], \quad (19)$$

and I is the $(2L+1)^2 \times (2L+1)^2$ identity matrix. Equation (18) is a polynomial equation of degree $(2L+1)^2$ for ω^2 . The roots of (18) gives the eigen-frequencies ω for a specified wave vector $\mathbf{k} = (k_x, k_y)$ in the first Brillouin zone (see Figure 3). The ranges of ω over which no real-valued wave vector \mathbf{k} exists are known as band gaps. It is seen from (19), (18), (16), (15), (13), (11), (10), (8), (6) and (2) that the value of ω depends on the material constants λ , μ , l , λ_0 , μ_0 , τ_0 and ρ , the foundation moduli k_w and k_p , and the geometrical parameters a , d and h .

The classical elasticity-based band gaps for flexural elastic wave propagation in the periodic composite plate structure resting on the Winkler–Pasternak elastic foundation can be obtained as a special case by setting $l = 0$ and $\lambda_0 = \mu_0 = \tau_0 = 0$ in (19).

3. Numerical results

To demonstrate the new model formulated in Section 2, sample cases are quantitatively studied here. In obtaining the numerical results presented in this section, Material *I* is chosen to be iron, whose properties are as follows (e.g., Gurtin and Murdoch 1978): for the bulk, Young's modulus $E^{(I)} = 177.33$ GPa, Poisson's ratio $\nu^{(I)} = 0.27$, $l^{(I)} = 6.76$ μm , $\rho = 7$ g/cm^3 ; for the surface layer, $\mu_0^{(I)} = 2.5$ N/m, $\lambda_0^{(I)} = -8$ N/m, $\tau_0^{(I)} = 1.7$ N/m. The value of $l^{(I)}$ above is determined from $l = b_h/\sqrt{3(1-\nu)}$ (e.g., Lam et al. 2003; Park and Gao 2006) with $\nu^{(I)} = 0.27$ and $b_h^{(I)} = 10$ μm (e.g., Wang 2010). Material *II* is taken to be epoxy with the following properties [Chen and Wang 2014]: $E^{(II)} = 3.3$ GPa, $\nu^{(II)} = 0.33$, $l^{(II)} = 16.93$ μm , $\rho^{(II)} = 1.18$ g/cm^3 for the bulk, and $\mu_0^{(II)} = 0.12406$ N/m, $\lambda_0^{(II)} = 0.16376$ N/m, $\tau_0^{(II)} = 0.045$ N/m for the surface layer. The value of $l^{(II)}$ given here is also calculated from $l = b_h/\sqrt{3(1-\nu)}$ but with $\nu^{(II)} = 0.33$ and $b_h^{(II)} = 24$ μm (e.g., Lam et al. 2003). The values of the surface elastic constants $\mu_0^{(II)}$ and $\lambda_0^{(II)}$ listed above are estimated using $\mu_0^{(II)} = \mu^{(II)}h^S$ and $\lambda_0^{(II)} = 2\lambda^{(II)}\mu^{(II)}h^S/(\lambda^{(II)} + \mu^{(II)})$ [Sharma and Ganti 2004], where h^S is the thickness of transition zone between the surface and bulk material and is taken to be 1 angstrom (e.g., Miller and Shenoy 2000), and $\lambda^{(II)}$ and $\mu^{(II)}$ are the Lamé

constants of the bulk epoxy given by $\lambda^{(II)} = E^{(II)}\nu^{(II)}/[(1+\nu^{(II)})(1-2\nu^{(II)})]$, $\mu^{(II)} = E^{(II)}/[2(1+\nu^{(II)})]$. In addition, $\tau_0^{(II)}$ is the surface tension for epoxy having a value of 45 mN/m (e.g., George 1993; Lewin et al. 2005). The foundation moduli k_w and k_p are non-dimensionalized to obtain $\bar{K}_w \equiv k_w a^4/D_C^{(I)}$, $\bar{K}_p \equiv k_p a^2/D_C^{(I)}$, with $D_C^{(I)} = E^{(I)}h^3/\{12[1 - (\nu^{(I)})^2]\}$ being the plate flexural rigidity of material I . Moreover, the edge length of the square inclusion is taken to be $d = 0.4a$ (i.e., $V_f^I = d^2/a^2 = 0.16$) in all the calculations for simplicity. In Figures 4–7, the blue dot lines represent the wave frequency curves obtained from solving (18). It has been found that a convergent solution is attained in each case with $L = 7$.

In the numerical results provided below, the first band gap in each case is defined to be that between the fourth and fifth frequency curves, which is first observed for the periodic composite plate structure without the elastic foundation (see Figure 4, left). This corresponds to the lowest range of ω that prohibits flexural wave propagation in the periodic composite plate structure without the foundation. In addition, the first band gap for the composite plate structure with the elastic foundation, called the first foundation band gap, is identified and discussed.

3.1. Effects of the elastic foundation. Figure 4 (left column, top) illustrates the first band gap frequency range for the periodic composite plate structure (with $a = 1$ mm and $h = 15$ μ m) predicted by the current non-classical model without including the foundation effect (i.e., $\bar{K}_w = 0$, $\bar{K}_p = 0$), which is 175.42 kHz–190.50 kHz (marked in orange) for the wave frequency $f = \omega/(2\pi)$. Figure 4 (left column, middle and bottom) displays the first band gap and the first foundation band gap frequency ranges predicted by the new non-classical model with the foundation treated as a Winkler one (i.e., setting $k_p = 0$): 177.33 kHz–192.17 kHz and 0 kHz–20.66 kHz for the case with $\bar{K}_w = 10$ and $\bar{K}_p = 0$; and 193.67 kHz–206.85 kHz and 0 kHz–62.97 kHz for the case with $\bar{K}_w = 100$ and $\bar{K}_p = 0$. Figure 4 (right column) shows the first band gap and the first foundation band gap for the composite plate structure predicted by the current non-classical model incorporating the Winkler–Pasternak foundation effect: 186.82 kHz–199.32 kHz and 0 kHz–20.69 kHz for the case with $\bar{K}_w = 10$ and $\bar{K}_p = 1$; 202.33 kHz–213.52 kHz and 0 kHz–63.18 kHz for the case with $\bar{K}_w = 100$ and $\bar{K}_p = 1$. For the case with $\bar{K}_w = 100$ and $\bar{K}_p = 10$, the first foundation band gap frequency range is 0 kHz–64.17 kHz, but no first band gap exists between the fourth and fifth frequency curves. However, a band gap is found between the first and second frequency curves, which is marked in green in Figure 4 (right column, bottom). This is called the second foundation band gap, which also exists in the cases with $\bar{K}_w = 100$ and $\bar{K}_p = 1$ and $\bar{K}_w = 100$ and $\bar{K}_p = 0$, as illustrated in Figure 4. Figure 4 shows the second foundation band gap frequency ranges predicted by the current non-classical model: 71.07 kHz–85.92 kHz for the case with $\bar{K}_w = 100$ and $\bar{K}_p = 0$; 74.68 kHz–89.57 kHz for the case with $\bar{K}_w = 100$ and $\bar{K}_p = 1$; and 100.54 kHz–117.30 kHz for the case with $\bar{K}_w = 100$ and $\bar{K}_p = 10$. From these frequency ranges, the band gaps can be readily determined, which are listed in Table 1.

From Figure 4 and Table 1, it is observed that the first band gap size decreases with the increase of either \bar{K}_w or \bar{K}_p . However, the first foundation band gap size increases with these two foundation moduli. Additionally, Figure 4 shows that the presence of either the Winkler–Pasternak foundation or the Winkler foundation reduces the first band gap size, and the effect of the former is more significant than that of the latter.

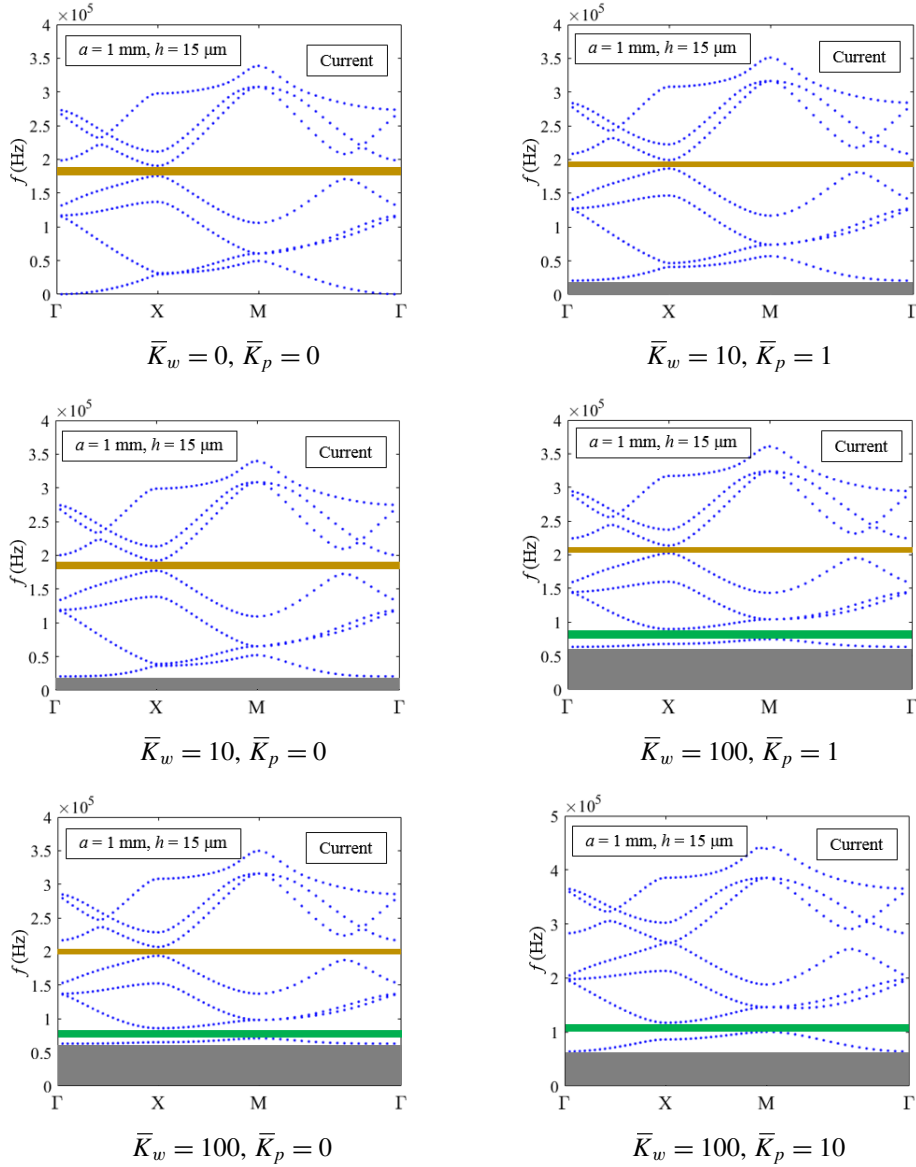


Figure 4. Band gaps for the periodic composite plate structure predicted by the current model. The Bloch wave vector $\mathbf{k} = (k_x, k_y)$ at Γ , X and M is, respectively, $(0, 0)$, $(\pi/a, 0)$ and $(\pi/a, \pi/a)$ (see Figure 3, right).

3.2. Effects of the microstructure and surface energy. Figure 5 displays the band gaps for the periodic composite plate structure predicted by the current model with $a = 1 \text{ mm}$, $\bar{K}_w = 10$, and $\bar{K}_p = 1$. Figure 5 (left column) shows the first band gap frequency ranges (in orange) and the first foundation band gap frequency ranges (in grey) predicted by the current non-classical model for different values of the plate thickness: 186.82 kHz–199.32 kHz and 0 kHz–20.69 kHz for $h = 15 \text{ }\mu\text{m}$; 322.81 kHz–355.31 kHz

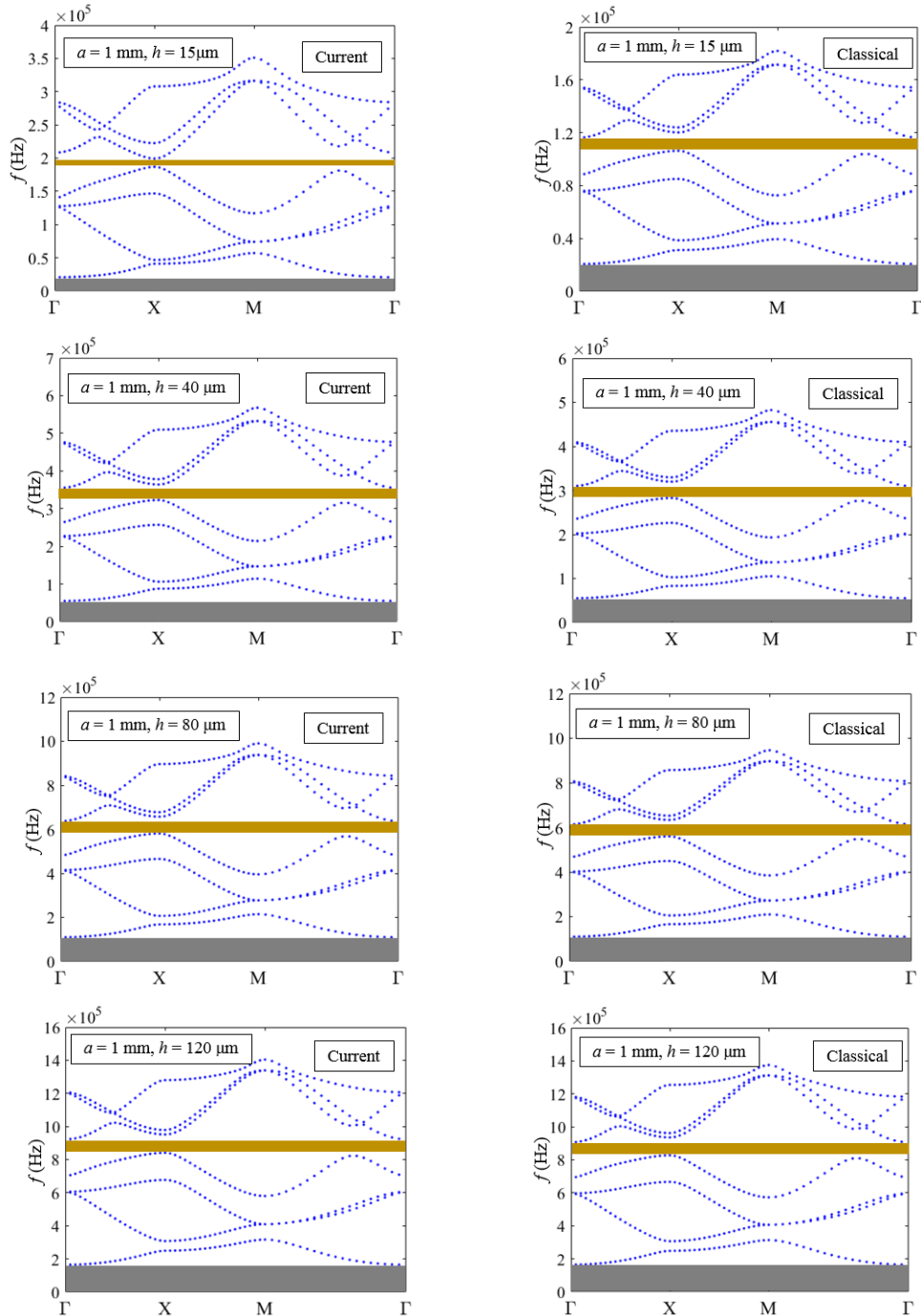


Figure 5. Band gaps for the periodic composite plate structure (with $a = 1$ mm, $\bar{K}_w = 10$ and $\bar{K}_p = 1$) predicted by the current model (left column) and the classical model (right column). The Bloch wave vector $\mathbf{k} = (k_x, k_y)$ at Γ , X and M is, respectively, $(0, 0)$, $(\pi/a, 0)$, and $(\pi/a, \pi/a)$ (see Figure 3, right).

Foundation moduli		First band gap (kHz)	First foundation band gap (kHz)	Second foundation band gap (kHz)
\bar{K}_w	\bar{K}_p			
0	0	15.08	NA	NA
10	0	14.84	20.66	NA
10	1	12.50	20.69	NA
100	0	13.18	62.97	14.85
100	1	11.19	63.18	14.89
100	10	NA	64.17	16.76

Table 1. Band gaps for the periodic composite plate structure with different values of the foundation moduli \bar{K}_w and \bar{K}_p predicted by the current model (with $a = 1$ mm, $h = 15$ μm).

h (μm)	Band gap (kHz)		Relative difference (%)
	Current model	Classical model	
15	12.50	10.22	22.31
40	32.50	27.22	19.40
80	56.98	54.20	5.13
120	82.58	80.70	2.33

Table 2. First band gaps for the periodic composite plate structure with different values of the plate thickness h .

and 0 kHz–55 kHz for $h = 40$ μm ; 581.07 kHz–638.05 kHz and 0 kHz–109.86 kHz for $h = 80$ μm ; and 841.20 kHz–923.78 kHz and 0 kHz–164.73 kHz for $h = 120$ μm .

Figure 5 (right column) illustrates the first band gap frequency ranges (in orange) and the first foundation band gap frequency ranges (in grey) predicted by the classical elasticity-based model for different values of the plate thickness: 106.28 kHz–116.50 kHz and 0 kHz–20.59 kHz for $h = 15$ μm ; 282.65 kHz–309.87 kHz and 0 kHz–54.9 kHz for $h = 40$ μm ; 560.00 kHz–614.20 kHz and 0 kHz–109.8 kHz for $h = 80$ μm ; and 827.20 kHz–907.90 kHz and 0 kHz–164.68 kHz for $h = 120$ μm . These frequency ranges give the two types of band gaps shown in Tables 2 and 3, respectively. In each case listed in Tables 2 and 3, the band gap value based on the classical model is used as the base value to compute the relative difference.

It is observed from Figure 5 and Table 2 that the first band gap size predicted by the current non-classical model is always larger than that predicted by the classical model. However, the difference between the two band gap sizes diminishes with the increase of the plate thickness h . When $h = 15$ μm , the band gap predicted by the current model is 1.22 times as large as that predicted by the classical model (with a relative difference of 22.31%). When $h = 120$ μm , the former is only 1.02 times of the latter, giving a relative difference of 2.33%. This shows that the effects of microstructure and surface energy on the first band gap are significant only for very thin plates.

Figure 5 and Table 3 reveal that the first foundation band gap predicted by the current non-classical model is always larger than that predicted by the classical model. However, the relative difference

h (μm)	Band gap (kHz) Current model	Band gap (kHz) Classical model	Relative difference (%)
15	20.69	20.59	0.49
40	55.00	54.90	0.18
80	109.86	109.80	0.05
120	164.73	164.68	0.03

Table 3. First foundation band gaps for the periodic composite plate structure with different values of the plate thickness h .

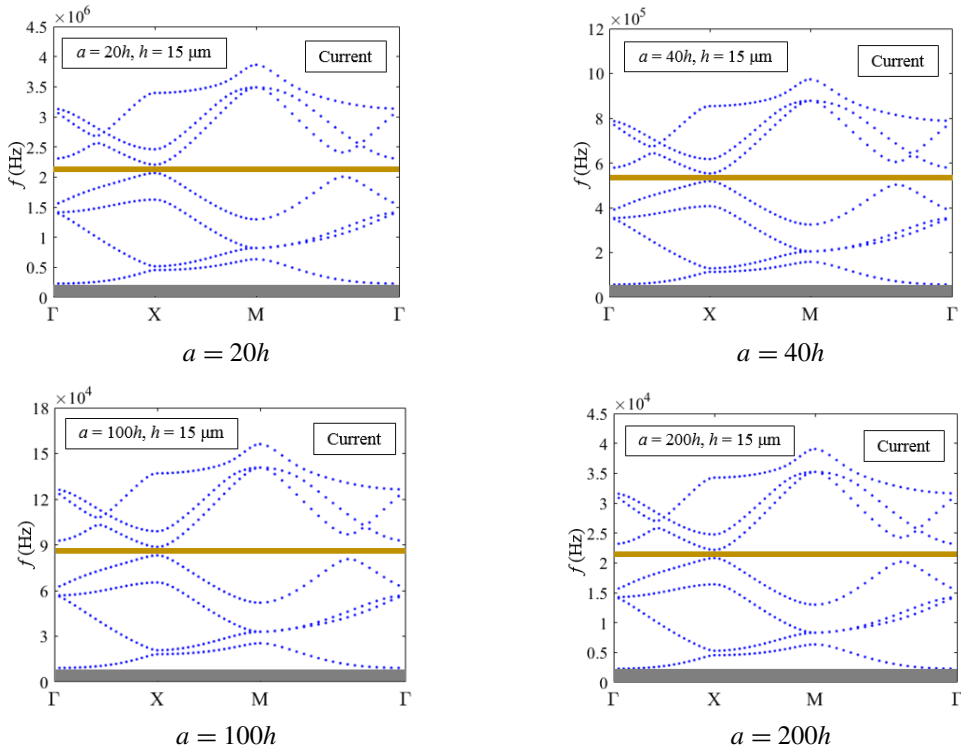


Figure 6. Band gaps for the periodic composite plate structure (with $h = 15 \mu\text{m}$, $\bar{K}_w = 10$ and $\bar{K}_p = 1$) predicted by the current model. The Bloch wave vector $\mathbf{k} = (k_x, k_y)$ at Γ , X and M is, respectively, $(0, 0)$, $(\pi/a, 0)$, and $(\pi/a, \pi/a)$ (see Figure 3, right).

decreases with the increase of the plate thickness h . In addition, this difference is negligibly small compared to the difference between the two first band gap values. This indicates that the effects of microstructure and surface energy on the first foundation band gap are insignificant even for very thin plates.

3.3. Effect of the unit cell length. Figure 6 illustrates the first band gap frequency ranges (in orange) and the first foundation band gap frequency ranges (in grey) for the periodic composite plate structure

a	First band gap (kHz)	First foundation band gap (kHz)
$20h$	138.7	229.89
$40h$	34.74	57.48
$100h$	5.56	9.20
$200h$	1.38	2.30

Table 4. Band gaps for the periodic composite plate structure with different values of the unit cell length a predicted by the current model (with $h = 15 \mu\text{m}$, $\bar{K}_w = 10$, and $\bar{K}_p = 1$).

a	First band gap (Hz)	First foundation band gap (Hz)
$20h$	1700	3431
$40h$	425.8	857.9
$100h$	68.15	137.26
$200h$	17.03	34.32

Table 5. Band gaps for the periodic composite plate structure with different values of the unit cell length a predicted by the current model (with $h = 1 \text{ mm}$, $\bar{K}_w = 10$, and $\bar{K}_p = 1$).

predicted by the current model for different values of the unit cell length a . The plate thickness is $h = 15 \mu\text{m}$, and the elastic foundation moduli are $\bar{K}_w = 10$ and $\bar{K}_p = 1$ in all cases.

The first band gap frequency range and the first foundation band gap frequency range are, respectively, 2065.9 kHz–2204.6 kHz and 0 kHz–229.89 kHz for the case with $a = 20h$ shown in Figure 6 (left column, top); 518.45 kHz–553.19 kHz and 0 kHz–57.48 kHz for the case with $a = 40h$ displayed in Figure 6 (right column, top); 83.07 kHz–88.63 kHz and 0 kHz–9.20 kHz for the case with $a = 100h$ depicted in Figure 6 (left column, bottom); and 20.80 kHz–22.18 kHz and 0 kHz–2.30 kHz for the case with $a = 200h$ illustrated in Figure 6 (right column, bottom). From these frequency ranges, the band gaps can be readily obtained, which are given in Table 4.

From Figure 6 and Table 4, it is observed that the frequency for producing the first band gap gets lower when the unit cell length a becomes larger and the sizes of the first band gap and the first foundation band gap decrease as a increases. The effect of the unit cell length is further illustrated in Figure 7.

Figure 7 shows the first band gap frequency ranges (in orange) predicted by the current model for the composite plate structure with $h = 1 \text{ mm}$, $\bar{K}_w = 10$, $\bar{K}_p = 1$ and different values of the unit cell length: 17639 Hz–19339 Hz for $a = 20h$, 4426.1 Hz–4851.9 Hz for $a = 40h$, 708.93 Hz–777.08 Hz for $a = 100h$, and 177.27 Hz–194.30 Hz for $a = 200h$. Also, Figure 7 displays the first foundation band gap frequency ranges for different values of the unit cell length: 0 kHz–3431 MHz, 0 kHz–857.9 MHz, 0 kHz–137.26 MHz and 0 kHz–34.32 MHz for the cases with $a = 20h$, $40h$, $100h$, and $200h$, respectively. From these frequency ranges, the band gaps are computed and given in Table 5.

From Figure 7 and Table 5, it is observed that both the frequency for producing the first band gap and the sizes of the first band gap and the first foundation band gap in the current cases with $h = 1 \text{ mm}$

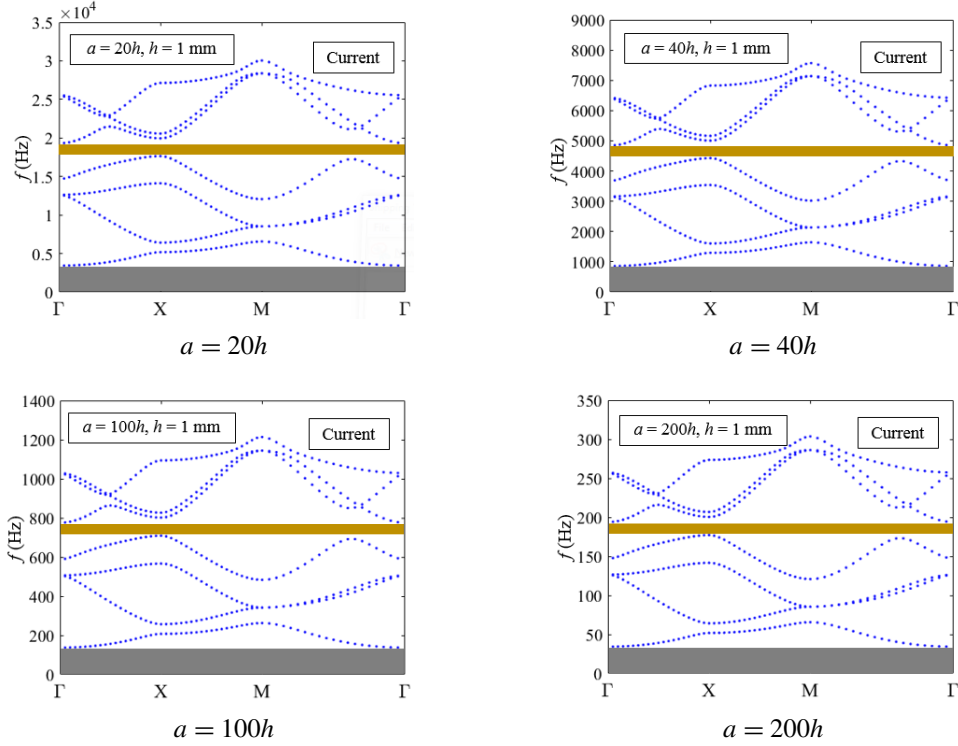


Figure 7. Band gaps for the periodic composite plate structure (with $h = 1$ mm, $\bar{K}_w = 10$ and $\bar{K}_p = 1$) predicted by the current model. The Bloch wave vector $\mathbf{k} = (k_x, k_y)$ at Γ , X and M is, respectively, $(0, 0)$, $(\pi/a, 0)$, and $(\pi/a, \pi/a)$ (see Figure 3, right).

decrease as the unit cell length a increases, which is the same trend as that seen from Figure 6 for the cases with $h = 15 \mu\text{m}$, a much smaller plate thickness. This shows that the effect of the unit cell length on band gaps exists at different length scales.

3.4. Effects of the volume fraction. The variations of the first band gap and the first foundation band gap with the volume fraction of material I (the inclusion phase) predicted by the current non-classical model are displayed in Figures 8 and 9, respectively. For comparison purposes, the variations predicted by the classical model are also shown in Figures 8 and 9. The numerical values for wave frequency plotted in Figures 8 and 9 are obtained from solving (18), with the convergent solution attained when $L = 7$ in each case. The properties adopted here for materials I and II are the same as those used to generate the numerical results displayed in Figures 4–7. In addition, $a = 1$ mm, $h = 15 \mu\text{m}$, $\bar{K}_w = 10$ and $\bar{K}_p = 1$ are employed in the calculations here.

From Figure 8, it is observed that the first band gap predicted by the current model starts at $V_f^{(I)} = 9.5\%$ and increases to its maximum of 13.82 kHz at $V_f^{(I)} = 20\%$, after which it decreases with $V_f^{(I)}$ until its disappearance at $V_f^{(I)} = 30\%$. Also, the first band gap predicted by the classical model increases from zero to its maximum value 13.31 kHz as $V_f^{(I)}$ goes from 9% to 21%, then it decreases with $V_f^{(I)}$ until vanishing at $V_f^{(I)} = 30\%$.

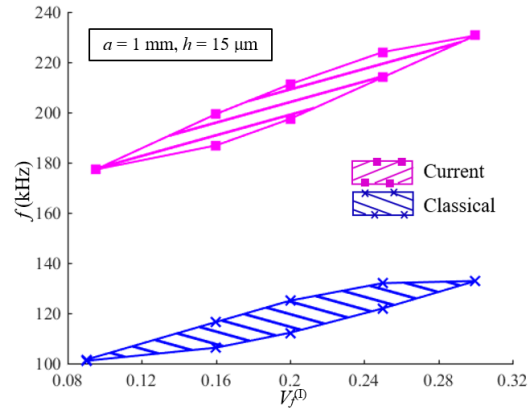


Figure 8. First band gap changing with $V_f^{(I)}$ predicted by the current and classical models for the periodic composite plate structure (with $a = 1$ mm, $h = 15$ μm , $\bar{K}_w = 10$ and $\bar{K}_p = 1$).

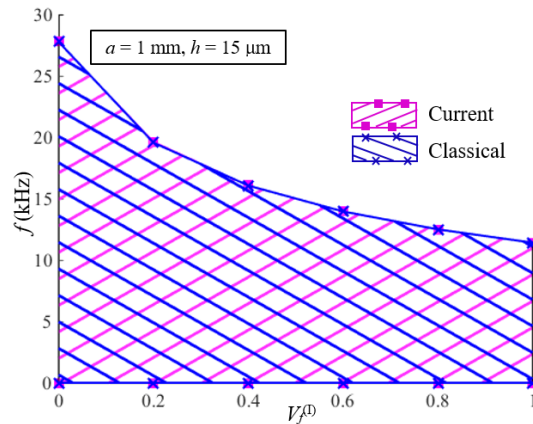


Figure 9. First foundation band gap changing with $V_f^{(I)}$ predicted by the current and classical models for the periodic composite plate structure (with $a = 1$ mm, $h = 15$ μm , $\bar{K}_w = 10$, and $\bar{K}_p = 1$).

From Figure 9, it is seen that the first foundation band gap predicted by the current non-classical model or the classical elasticity-based model gradually decreases with the increase of $V_f^{(I)}$ from 0% to 100%. Also, it is observed that the first foundation band gap values predicted by the current non-classical model and those predicted by the classical model are very close, thereby indicating that the effects of microstructure and surface energy on the first foundation band gap are not significant. This agrees with what is observed from Figure 5 and Table 3.

From Figures 8 and 9, it is clear that the volume fraction does have a significant effect on the first band gap and the first foundation band gap for the periodic composite plate structure according to both the current non-classical and the classical models. This shows that large band gaps can be generated by adjusting the volume fraction of the inclusion phase.

4. Summary

A new model is provided for determining elastic wave band gaps in a periodic composite plate structure. It is based on a non-classical Kirchhoff plate model, the plane wave expansion method and the Bloch theorem. The current non-classical model recovers the classical model as a special case after neglecting the microstructure and surface energy effects. The new model simultaneously incorporates the microstructure, surface energy and elastic foundation effects for the first time. In addition, the band gaps predicted by the current model vary with the unit cell size and volume fraction of the inclusion phase.

Numerical results show that the first band gap predicted by the current model including the foundation effect is smaller than that without considering this effect, and the first foundation band gap increases with the elastic foundation moduli. In addition, the first band gap predicted by the new non-classical model is seen to be always larger than that based on the classical model, with the difference being significant for very thin plates. It is also observed that the first band gap frequency and the sizes of the first band gap and the first foundation band gap decrease with the increase of the unit cell length. Finally, it is found that the volume fraction has a significant effect on the band gap size, indicating that large band gaps can be achieved by tailoring the volume fraction.

References

- [Bacigalupo and Gambarotta 2017] A. Bacigalupo and L. Gambarotta, “Dispersive wave propagation in two-dimensional rigid periodic blocky materials with elastic interfaces”, *J. Mech. Phys. Solids* **102** (2017), 165–186.
- [Cao et al. 2004] Y. Cao, Z. Hou, and Y. Liu, “Convergence problem of plane-wave expansion method for phononic crystals”, *Phys. Lett. A* **327** (2004), 247–253.
- [Chen and Wang 2014] Y. Chen and L. Wang, “Periodic co-continuous acoustic metamaterials with overlapping locally resonant and Bragg band gaps”, *Appl. Phys. Lett.* **105**:19 (2014), article id 191907 (5 pages).
- [Chen et al. 2017] Y. Chen, T. Li, F. Scarpa, and L. Wang, “Lattice metamaterials with mechanically tunable Poisson’s ratio for vibration control”, *Phys. Rev. Appl.* **7**:2 (2017), article id 024012 (11 pages).
- [Gao and Park 2007] X.-L. Gao and S. K. Park, “Variational formulation of a simplified strain gradient elasticity theory and its application to a pressurized thick-walled cylinder problem”, *Int. J. Solids Struct.* **44**:22-23 (2007), 7486–7499.
- [Gao and Zhang 2016] X.-L. Gao and G. Y. Zhang, “A non-classical Kirchhoff plate model incorporating microstructure, surface energy and foundation effects”, *Contin. Mech. Therm.* **28**:1-2 (2016), 195–213.
- [Gao et al. 2018] R. Z. Gao, G. Y. Zhang, T. Ioppolo, and X.-L. Gao, “Elastic wave propagation in a periodic composite beam structure: a new model for band gaps incorporating surface energy, transverse shear and rotational inertia effects”, *J. Micromech. Molecular Phys.* **3** (2018), article id 1840005 (22 pages).
- [George 1993] G. A. George, “Surface modification and analysis of ultra-high-modulus polyethylene fibres for composites”, pp. 161–201, in *Polymer surfaces and interfaces*, vol. II, edited by W. J. Feast et al., Wiley, Chichester, England, 1993.
- [Gurtin and Murdoch 1975] M. E. Gurtin and A. I. Murdoch, “A continuum theory of elastic material surfaces”, *Arch. Ration. Mech. Anal.* **57**:4 (1975), 291–323.
- [Gurtin and Murdoch 1978] M. E. Gurtin and A. I. Murdoch, “Surface stress in solids”, *Int. J. Solids Struct.* **14**:6 (1978), 431–440.
- [Kittel 1986] C. Kittel, *Introduction to solid state physics*, Wiley, New York, 1986.
- [Lam et al. 2003] D. C. C. Lam, F. Yang, A. C. M. Chong, J. Wang, and P. Tong, “Experiments and theory in strain gradient elasticity”, *J. Mech. Phys. Solids* **51**:8 (2003), 1477–1508.
- [Lewin et al. 2005] M. Lewin, A. Mey-Marom, and R. Frank, “Surface free energies of polymeric materials, additives and minerals”, *Polym. Adv. Technol.* **16** (2005), 429–441.

- [Li 1996] L. Li, “Use of Fourier series in the analysis of discontinuous periodic structures”, *J. Opt. Soc. Am. A* **13** (1996), 1870–1876.
- [Li et al. 2016] Y. Li, P. Wei, and Y. Zhou, “Band gaps of elastic waves in 1-D phononic crystal with dipolar gradient elasticity”, *Acta Mech.* **227**:4 (2016), 1005–1023.
- [Liu and Hussein 2012] L. Liu and M. I. Hussein, “Wave motion in periodic flexural beams and characterization of the transition between Bragg scattering and local resonance”, *J. Appl. Mech. (ASME)* **79**:1 (2012), article id 011003 (17 pages).
- [Liu et al. 2012] W. Liu, J. Chen, Y. Liu, and X. Su, “Effect of interface/surface stress on the elastic wave band structure of two-dimensional phononic crystals”, *Phys. Lett. A* **376**:4 (2012), 605–609.
- [Madeo et al. 2016] A. Madeo, G. Barbagallo, M. V. d’Agostino, L. Placidi, and P. Neff, “First evidence of non-locality in real band-gap metamaterials: determining parameters in the relaxed micromorphic model”, *Proc. Royal Soc. Lond. A* **472** (2016), article id 20160169 (21 pages).
- [Maranganti and Sharma 2007] R. Maranganti and P. Sharma, “A novel atomistic approach to determine strain-gradient elasticity constants: Tabulation and comparison for various metals, semiconductors, silica, polymers and the (ir) relevance for nanotechnologies”, *J. Mech. Phys. Solids* **55**:9 (2007), 1823–1852.
- [Mi et al. 2008] C. Mi, S. Jun, D. A. Kouris, and S. Y. Kim, “Atomistic calculations of interface elastic properties in noncoherent metallic bilayers”, *Phys. Rev. B* **77**:7 (2008), article id 075425 (12 pages).
- [Miller and Shenoy 2000] R. E. Miller and V. B. Shenoy, “Size-dependent elastic properties of nanosized structural elements”, *Nanotechnology* **11**:3 (2000), 139–147.
- [Mindlin 1963] R. D. Mindlin, “Influence of couple-stresses on stress concentrations”, *Exp. Mech.* **3**:1 (1963), 1–7.
- [Park and Gao 2006] S. K. Park and X.-L. Gao, “Bernoulli–Euler beam model based on a modified couple stress theory”, *J. Micromech. Microeng.* **16**:11 (2006), 2355–2359.
- [Park and Gao 2008] S. K. Park and X.-L. Gao, “Variational formulation of a modified couple stress theory and its application to a simple shear problem”, *Z. Angew. Math. Phys.* **59**:5 (2008), 904–917.
- [Piccolroaz and Movchan 2014] A. Piccolroaz and A. B. Movchan, “Dispersion and localisation in structured Rayleigh beams”, *Int. J. Solids Struct.* **51**:25-26 (2014), 4452–4461.
- [Piccolroaz et al. 2017] A. Piccolroaz, A. B. Movchan, and L. Cabras, “Rotational inertia interface in a dynamic lattice of flexural beams”, *Int. J. Solids Struct.* **112** (2017), 43–53.
- [Sharma and Ganti 2004] P. Sharma and S. Ganti, “Size-dependent Eshelby’s tensor for embedded nano-inclusions incorporating surface/interface energies”, *J. Appl. Mech. (ASME)* **71**:5 (2004), 663–671.
- [Shodja et al. 2012] H. M. Shodja, F. Ahmadpoor, and A. Tehranchi, “Calculation of the additional constants for fcc materials in second strain gradient elasticity: behavior of a nano-size Bernoulli–Euler beam with surface effects”, *J. Appl. Mech. (ASME)* **79**:2 (2012), article id 021008 (8 pages).
- [Sigalas 1997] M. M. Sigalas, “Elastic wave band gaps and defect states in two-dimensional composites”, *J. Acoust. Soc. Am.* **101**:3 (1997), 1256–1261.
- [Sigalas and Economou 1994] M. M. Sigalas and E. N. Economou, “Elastic waves in plates with periodically placed inclusions”, *J. Appl. Phys.* **75**:6 (1994), 2845–2850.
- [Steigmann and Ogden 1997] D. J. Steigmann and R. W. Ogden, “Plane deformations of elastic solids with intrinsic boundary elasticity”, *Proc. Royal Soc. Lond. A* **453**:1959 (1997), 853–877.
- [Steigmann and Ogden 1999] D. J. Steigmann and R. W. Ogden, “Elastic surface-substrate interactions”, *Proc. Royal Soc. Lond. A* **455**:1982 (1999), 437–474.
- [Susa 2002] N. Susa, “Large absolute and polarization-independent photonic band gaps for various lattice structures and rod shapes”, *J. Appl. Phys.* **91**:6 (2002), 3501–3510.
- [Wang 2010] L. Wang, “Size-dependent vibration characteristics of fluid-conveying microtubes”, *J. Fluid. Struct.* **26**:4 (2010), 675–684.
- [Xiao et al. 2012] Y. Xiao, J. Wen, and X. Wen, “Flexural wave band gaps in locally resonant thin plates with periodically attached spring-mass resonators”, *J. Phys. D Appl. Phys.* **45**:19 (2012), article id 195401 (12 pages).

- [Yang et al. 2002] F. Yang, A. C. M. Chong, D. C. C. Lam, and P. Tong, “Couple stress based strain gradient theory for elasticity”, *Int. J. Solids Struct.* **39**:10 (2002), 2731–2743.
- [Yokoyama 1996] T. Yokoyama, “Vibration analysis of Timoshenko beam-columns on two-parameter elastic foundations”, *Comput. Struct.* **61**:6 (1996), 995–1007.
- [Zhang and Gao 2018] G. Y. Zhang and X.-L. Gao, “Elastic wave propagation in 3-D periodic composites: band gaps incorporating microstructure effects”, *Compos. Struct.* **204** (2018), 920–932.
- [Zhang and Parnell 2017] P. Zhang and W. J. Parnell, “Band gap formation and tunability in stretchable serpentine interconnects”, *J. Appl. Mech. (ASME)* **84**:9 (2017), article id 091007 (7 pages).
- [Zhang and Zhao 2016] Y. Zhang and Y.-P. Zhao, “Measuring the nonlocal effects of a micro/nanobeam by the shifts of resonant frequencies”, *Int. J. Solids Struct.* **102-103** (2016), 259–266.
- [Zhang et al. 2018a] G. Y. Zhang, X.-L. Gao, J. E. Bishop, and H. E. Fang, “Band gaps for elastic wave propagation in a periodic composite beam structure incorporating microstructure and surface energy effects”, *Compos. Struct.* **189** (2018), 263–272.
- [Zhang et al. 2018b] G. Y. Zhang, X.-L. Gao, and S. R. Ding, “Band gaps for wave propagation in 2-D periodic composite structures incorporating microstructure effects”, *Acta Mech.* **229**:10 (2018), 4199–4214.

Received 20 Oct 2018. Accepted 25 Dec 2018.

GONGYE ZHANG: gyzhang@seu.edu.cn

Jiangsu Key Laboratory of Engineering Mechanics, School of Civil Engineering, Southeast University, Nanjing, Jiangsu, China

XIN-LIN GAO: xlgao@smu.edu

Department of Mechanical Engineering, Southern Methodist University, Dallas, TX, United States

JOURNAL OF MECHANICS OF MATERIALS AND STRUCTURES

msp.org/jomms

Founded by Charles R. Steele and Marie-Louise Steele

EDITORIAL BOARD

ADAIR R. AGUIAR	University of São Paulo at São Carlos, Brazil
KATIA BERTOLDI	Harvard University, USA
DAVIDE BIGONI	University of Trento, Italy
MAENGHYO CHO	Seoul National University, Korea
HUILING DUAN	Beijing University
YIBIN FU	Keele University, UK
IWONA JASLUK	University of Illinois at Urbana-Champaign, USA
DENNIS KOCHMANN	ETH Zurich
MITSUTOSHI KURODA	Yamagata University, Japan
CHEE W. LIM	City University of Hong Kong
ZISHUN LIU	Xi'an Jiaotong University, China
THOMAS J. PENCE	Michigan State University, USA
GIANNI ROYER-CARFAGNI	Università degli studi di Parma, Italy
DAVID STEIGMANN	University of California at Berkeley, USA
PAUL STEINMANN	Friedrich-Alexander-Universität Erlangen-Nürnberg, Germany
KENJIRO TERADA	Tohoku University, Japan

ADVISORY BOARD

J. P. CARTER	University of Sydney, Australia
D. H. HODGES	Georgia Institute of Technology, USA
J. HUTCHINSON	Harvard University, USA
D. PAMPLONA	Universidade Católica do Rio de Janeiro, Brazil
M. B. RUBIN	Technion, Haifa, Israel

PRODUCTION production@msp.org

SILVIO LEVY Scientific Editor

Cover photo: Mando Gomez, www.mandolux.com

See msp.org/jomms for submission guidelines.

JoMMS (ISSN 1559-3959) at Mathematical Sciences Publishers, 798 Evans Hall #6840, c/o University of California, Berkeley, CA 94720-3840, is published in 10 issues a year. The subscription price for 2019 is US \$635/year for the electronic version, and \$795/year (+\$60, if shipping outside the US) for print and electronic. Subscriptions, requests for back issues, and changes of address should be sent to MSP.

JoMMS peer-review and production is managed by EditFLOW® from Mathematical Sciences Publishers.

PUBLISHED BY

 **mathematical sciences publishers**
nonprofit scientific publishing

<http://msp.org/>

© 2019 Mathematical Sciences Publishers

Journal of Mechanics of Materials and Structures

Volume 14, No. 2

March 2019

- A mode-dependent energy-based damage model for peridynamics and its implementation**
CHRISTIAN WILLBERG, LASSE WIEDEMANN and MARTIN RÄDEL 193
- Elastic wave propagation in a periodic composite plate structure: band gaps incorporating microstructure, surface energy and foundation effects**
GONGYE ZHANG and XIN-LIN GAO 219
- Dynamic analysis of a mass traveling on a simply supported nonhomogeneous beam composed of transversely embedded periodic arrays**
YI-MING WANG and HUNG-CHIEH LIU 237
- Stress concentration around an arbitrarily-shaped hole in nonlinear fully coupled thermoelectric materials**
CHUAN-BIN YU, HAI-BING YANG, KUN SONG and CUN-FA GAO 259
- The effect of variable thermal conductivity on an infinite fiber-reinforced thick plate under initial stress**
MOHAMED I. A. OTHMAN, AHMED E. ABOUELREGAL and SAMIA M. SAID 277
- Large deflections and stability of spring-hinged cantilever beam** MILAN BATISTA 295



1559-3959(2019)14:2;1-W